Cavity-assisted cooling of a trapped atom using cavity-induced transparency

Shuo Zhang,[1] Qian-Heng Duan,[1] Chu Guo,[1] Chun-Wang Wu,[1] Wei Wu,[1,2] and Ping-Xing Chen[1,2,*]
[1]*College of Science, National University of Defense Technology, Changsha 410073, P. R. China*
[2]*State Key Laboratory of High Performance Computing, National University of Defense Technology, Changsha 410073, P. R. China*
(Received 31 May 2013; published 6 January 2014)

We investigate the cooling dynamics of a trapped Λ-configuration atom coupling to a high-finesse cavity. We find that the heating effects due to diffusion and heating transitions can be simultaneously suppressed by the cavity-induced transparency and the electromagnetically induced transparency effects, respectively. Compared to the current cavity cooling schemes, the trapped atom in our scheme can be cooled to a relatively lower final temperature.

DOI: 10.1103/PhysRevA.89.013402 PACS number(s): 37.10.De, 03.67.Lx, 42.50.−p

I. INTRODUCTION

Cooling of a trapped atom to its motional ground state is an important step towards quantum technological applications [1]. The first effective ground state cooling scheme of trapped systems is sideband cooling [2,3], which is achieved by tuning the cooling laser in resonance with the red sideband transition. Meanwhile, the final temperature is limited by two dominant heating effects: the diffusion due to the population of atomic excitation and the off-resonant blue sideband heating transition. To further enhance the cooling efficiency, a variety of cooling schemes have been proposed in recent years, including using dark state [4–7], by means of an optical cavity [8–16], etc. [17,18].

Cooling in an optical cavity has proven to be an effective way to achieve a low temperature [19–22]. The cavity cooling schemes usually rely on strong coupling, which means that the cooperativity C should satisfy

$$C = \frac{\tilde{g}^2}{\kappa\gamma} \gg 1, \tag{1}$$

where $\tilde{g}$ is the effective atom-cavity coupling strength, 2κ is the cavity decay rate, and 2γ is the atomic spontaneous emission rate. There are two kinds of cavity cooling methods: the cavity sideband cooling and the cavity coherent cooling.

Cavity sideband cooling [9,20,23,24], which is similar to the sideband cooling in free space, is carried out by tuning the cooling laser into resonance with the red sideband of the cavity excitation. The final phonon number is predicted to be

$$\langle n\rangle_{ss} = \left(\frac{\kappa}{2\nu}\right)^2 + O\left(\frac{1}{C}\right), \tag{2}$$

where ν is the trap frequency.

Cavity coherent cooling [8–13,16], on the other hand, has been proposed to overcome the heating effects. In such schemes, the heating effects can be suppressed due to the quantum destructive interference between the heating pathways, giving rise to a lower final temperature than cavity sideband cooling. There are several quantum coherent cooling methods, one of which is achieved by a two-photon resonance, which is also known as the cavity-induced transparency (CIT) effect [25], in a high-finesse cavity. In analogy with electromagnetically induced transparency (EIT) effect in free space [26], when the cooling laser and cavity are resonant, CIT arises so that the atomic excitation is nearly absent. Therefore, the diffusion is almost vanishes [9]. Another cooling method [12] is achieved by a three-photon resonance, namely, the cavity-induced EIT. In cavity-induced EIT cooling, not only the diffusion is eliminated, but also the heating transition can be partly suppressed, and the analytical prediction of the final phonon number is of the order

$$\langle n\rangle_{ss} \sim O\left(\frac{1}{C}\right). \tag{3}$$

In a recent work [16], the authors proposed an improved cavity-induced EIT cooling scheme by employing the property of the cavity standing wave. In this scheme, the diffusion is canceled by precisely locating the atom at the node of the cavity standing wave, and the heating transitions are eliminated by the cavity-induced EIT. Thus all the heating effects vanish, and the cooling efficiency can be further enhanced.

In this work, we present an alternative ground state cooling scheme of a trapped atom in an optical cavity. We investigate the cooling dynamics of a Λ configuration three-level atom coupling with two laser fields and a high-finesse optical cavity and find that the diffusion and heating transition can be strongly suppressed by the combination of the CIT and EIT effects. The analytical result shows that the final phonon number of the new scheme can be

$$\langle n\rangle_{ss} < O\left(\frac{1}{C^2} + \frac{\kappa^4}{\nu^4}\right). \tag{4}$$

Further numerical simulation shows that our scheme can be much lower than previous cavity cooling schemes and the same order as Ref. [16].

II. MODEL

The experimental setup is shown in Fig. 1(a), and the atomic-level configuration is shown in Fig. 1(b). An atom of mass M is confined by a one-dimensional harmonic trap inside an optical cavity with the decay rate 2κ. The trap frequency is ν. The internal levels of the atom are in the Λ configuration: the dissipative upper state $|e\rangle$ with level frequency ω_e and decay rate 2γ, which can be coupled to two ground states by dipole transitions: $|g\rangle$ with level frequency ω_g and $|r\rangle$ with level

*pxchen@nudt.edu.cn

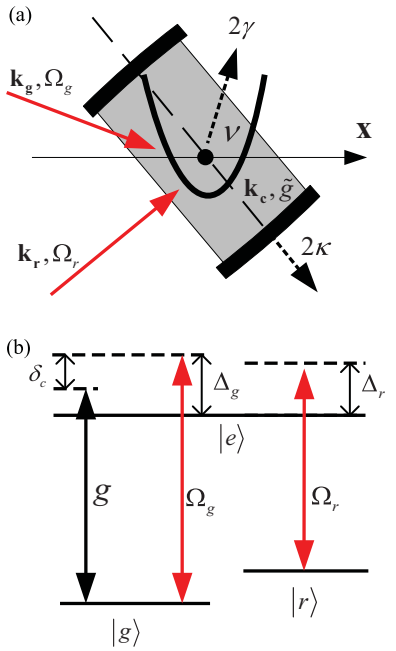

FIG. 1. (Color online) (a) A Λ-configuration atom is inside an optical cavity. The atom is coupled with two laser fields and the cavity field. The system is dissipated by the cavity photon leak or atom spontaneous emission. (b) The atom has an excited state $|e\rangle$ and two ground states $|g\rangle$ and $|r\rangle$; $|e\rangle \leftrightarrow |g\rangle$ is driven by a "cooling" laser and cavity field, and $|e\rangle \leftrightarrow |r\rangle$ is driven by a "coupling" laser; the detunings of the coupling are defined by Eq. (7).

frequency ω_r. The atom is coupled by two laser beams and one cavity mode. The transition $|e\rangle \leftrightarrow |g\rangle$ is driven by both a "cooling" laser beam with the frequency ω_{L1}, Rabi frequency Ω_g, and the cavity mode with the frequency ω_c and strength g. The transition $|e\rangle \leftrightarrow |r\rangle$ is driven by another "coupling" laser beam with the frequency ω_{L2} and Rabi frequency Ω_r. Here we take into account the geometry setup of the laser and cavity fields and the motional axis, as illustrated in Fig. 1(a).

The Hamiltonian of the system is given by

$$H = H_0 + H_I. \tag{5}$$

H_0 is the free Hamiltonian for the atomic levels and the phonon and cavity mode, which is ($\hbar = 1$)

$$H_0 = \nu b^\dagger b - \delta_c a^\dagger a - \Delta_g |e\rangle\langle e| - (\Delta_g - \Delta_r)|r\rangle\langle r|. \tag{6}$$

In this paper the Hamiltonians are described in the reference frame rotating at the laser frequency ω_{L1}. a and b are the annihilation operators of a cavity photon and a phonon, respectively. The detunings are defined by

$$\begin{aligned} \delta_c &= \omega_{L1} - \omega_c, \quad \Delta_g = \omega_{L1} - (\omega_e - \omega_g), \\ \Delta_r &= \omega_{L2} - (\omega_e - \omega_r). \end{aligned} \tag{7}$$

H_I describes the interactions between the atom and the laser and cavity fields:

$$\begin{aligned} H_I = \Bigg[& ga \sin(\boldsymbol{k_c} \cdot \boldsymbol{x} + \phi)|e\rangle\langle g| + \frac{\Omega_g}{2} e^{-i\boldsymbol{k_{L1}}\cdot\boldsymbol{x}}|e\rangle\langle g| \\ & + \frac{\Omega_r}{2} e^{-i\boldsymbol{k_{L2}}\cdot\boldsymbol{x}}|e\rangle\langle r| \Bigg] + \text{H.c.}, \end{aligned} \tag{8}$$

where $\boldsymbol{k_c}$, $\boldsymbol{k_{L1}}$, and $\boldsymbol{k_{L2}}$ are the wave vectors of the cavity and two laser beams; ϕ denotes the phase of the standing wave in the cavity, and $\boldsymbol{x}$ is the position of the atom. In particular, $\phi = 0$ corresponds to the atom located at the node of the standing wave, while $\phi = \frac{\pi}{2}$ indicates the atom at antinode.

Our cooling scheme focuses on the Lamb-Dicke (LD) regime, which means that the size of the atom's motional wave packet is much smaller than the wavelength of the lasers. In the LD regime, the internal and motional degrees of freedom (DOF) are weakly coupled, and the internal DOF can be adiabatically eliminated as a steady state. So it is necessary to analyze the dynamics of the internal DOF, which consist of the atomic DOF and cavity mode. In our scheme we assume that the coupling strength of the "cooling" laser is sufficiently weak, i.e., $\Omega_g \ll \max\{|\Delta_g|, \gamma\}$. Meanwhile, the coupling strengths of the cavity field and "coupling" laser are much stronger than Ω_g:

$$\Omega_g \ll \Omega_r, \tilde{g}, \tag{9}$$

with the effective coupling strength $\tilde{g}$ defined by $\tilde{g} = g \sin\phi$. Under these assumptions, the internal steady state is almost at $|g,0_c\rangle$, where the notation m_c is the mth Fock state of the cavity. Starting from the internal ground state $|g,0_c\rangle$, the internal DOF can be weakly excited to state $|e,0_c\rangle$, which couples to the states $|g,1_c\rangle$ and $|r,0_c\rangle$ by the cavity field and "coupling" laser, respectively. State $|g,1_c\rangle$ may also be weakly excited to state $|e,1_c\rangle$, but the scattering process from $|g,0_c\rangle$ to $|e,1_c\rangle$ involves two weak transitions, which can be neglected. Therefore, we can only consider that the internal DOF take place among the space which is spanned by the states

$$\{|g,0_c\rangle, |g,1_c\rangle, |r,0_c\rangle, |e,0_c\rangle\}. \tag{10}$$

Note the truncated internal DOF (10) is equivalent to a four-level system. Then we divide the internal DOF (10) into two subspaces: the steady state or ground state $|g,0_c\rangle$ and the excited subspace, which is spanned by the basis of states $\{|g,1_c\rangle, |r,0_c\rangle, |e,0_c\rangle\}$. In the LD regime, the Hamiltonian (5) is

$$H_{\text{LD}} = H_e + V_0 + V_1, \tag{11}$$

where H_e describes the Hamiltonian of the phonon state and excited subspace:

$$\begin{aligned} H_e = {} & \nu b^\dagger b - \delta_c a^\dagger a - \Delta_g |e\rangle\langle e| - (\Delta_g - \Delta_r)|r\rangle\langle r| \\ & + \tilde{g}(a|e\rangle\langle g| + a^\dagger |g\rangle\langle e|) + \frac{\Omega_r}{2}\sigma_x^r. \end{aligned} \tag{12}$$

V_0 is the optical pumping from the internal ground state to the excited subspace including the carrier transition and the sideband transitions:

$$\begin{aligned} V_0 &= V_0^0 + V_0^1, \\ V_0^0 &= \frac{\Omega_g}{2}\sigma_x^g, \\ V_0^1 &= \eta_g \frac{\Omega_g}{2}(b^\dagger + b)\sigma_y^g. \end{aligned} \tag{13}$$

V_1 describes the sideband transitions among the excited states

$$V_1 = \eta_c\tilde{g}(a|e\rangle\langle g| + a^\dagger|g\rangle\langle e|)(b+b^\dagger) + \eta_r\frac{\Omega_r}{2}(b^\dagger+b)\sigma_y^r, \tag{14}$$

where $\sigma_x^j = |e\rangle\langle j| + |j\rangle\langle e|$, $\sigma_y^j = (|e\rangle\langle j| - |j\rangle\langle e|)/i$ $(j = g,r)$ and the effective LD parameters are defined by

$$\eta_g = \boldsymbol{k_{L1}}\cdot\boldsymbol{e_x}\sqrt{\frac{1}{2M\nu}},$$
$$\eta_r = \boldsymbol{k_{L2}}\cdot\boldsymbol{e_x}\sqrt{\frac{1}{2M\nu}}, \tag{15}$$
$$\eta_c = \boldsymbol{k_c}\cdot\boldsymbol{e_x}\sqrt{\frac{1}{2M\nu}}\cot\phi.$$

Here the angles between the directions of the optical fields and the motional direction are included in the effective LD parameters. In particular, if the direction of the optical field is perpendicular to the motional axis, $\eta = 0$, indicating that no heating and cooling effects along the motional direction.

In the following, we restrict ourselves to the good cavity limit, which means the cavity loss rate is small and the coupling is strong:

$$\kappa \ll \nu,\gamma,\tilde{g}, \quad C = \frac{\tilde{g}^2}{\kappa\gamma} \gg 1. \tag{16}$$

In our scheme, we employ the EIT and CIT effects to suppress the heating effects, which is shown in Fig. 2. Starting from nth phonon steady state $|g,0_c,n\rangle$, all the dominant heating processes include either the carrier transition $|g,0_c,n\rangle \to |e,0_c,n\rangle$ or blue sideband transition $|g,0_c,n\rangle \to |e,0_c,n+1\rangle$. If we set the detuning

$$\delta_c = 0, \tag{17}$$

then the CIT effect arises and the scattering amplitude of carrier transition can be suppressed by the transition $|g,1_c,n\rangle \to |e,0_c,n\rangle$. By further setting the detunings

$$\Delta_g - \Delta_r - \nu = 0, \tag{18}$$

the EIT effect arises between the transitions $|g,0_c,n\rangle \to |e,0_c,n+1\rangle$ and $|r,0_c,n+1\rangle \to |e,0_c,n+1\rangle$, and therefore the blue sideband heating is eliminated. In the ideal case that the cavity is lossless, i.e., $\kappa = 0$, the two heating transitions

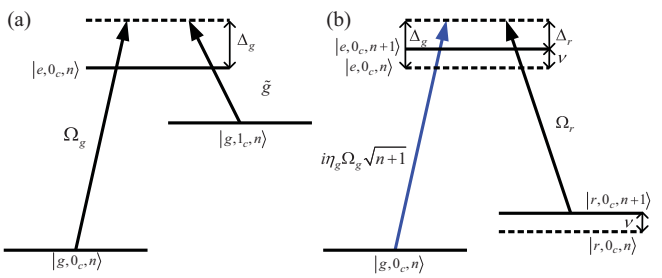

FIG. 2. (Color online) Suppression of the heating transitions. (a) The carrier transition $|g,0_c,n\rangle \to |e,0_c,n\rangle$ is suppressed by the transition $|g,1_c,n\rangle \to |e,0_c,n\rangle$ by the CIT effect. (b) The blue sideband transition $|g,0_c,n\rangle \to |e,0_c,n+1\rangle$ is eliminated by the transition $|r,0_c,n+1\rangle \to |e,0_c,n+1\rangle$ by the EIT effect.

are exactly eliminated, and the whole system will be cooled to the unnormalized dark state:

$$|\Psi\rangle \approx \Omega_r(2\tilde{g}|g,0_c,0\rangle - \Omega_g|g,1_c,0\rangle) + i\eta_g 2\Omega_g\tilde{g}|r,0_c,1\rangle + O(\eta^2). \tag{19}$$

For finite cavity loss rate κ, the carrier transition still exists, and we can calculate the cooling result by the rate equation, as shown in the next section.

III. ANALYTICAL RESULT

In this section we analytically calculate the cooling dynamics.

The dynamics of the whole system is determined by the master equation, which reads

$$\frac{d\rho}{dt} = -i[H,\rho] + \sum_{j=g,r}\gamma_j \times\left\{|j\rangle\langle e|\left[2\int_{-1}^{1}\mathcal{N}_j(\theta)e^{ik_jx\cos\theta}\rho e^{-ik_jx\cos\theta}\,d\cos\theta\right]|e\rangle\langle j| - |e\rangle\langle e|\rho - \rho|e\rangle\langle e|\right\} + \kappa(2a\rho a^\dagger - a^\dagger a\rho - \rho a^\dagger a), \tag{20}$$

where $k_j = (\omega_e - \omega_j)/c$, $2\gamma_j$ is the rate of spontaneous emission from state $|e\rangle$ to state $|j\rangle$ and $\mathcal{N}_j(\theta)$ is the corresponding angular distribution function of the emitted photons $(j = g,r)$. Here we choose

$$\mathcal{N}_j(\theta) = \tfrac{3}{4}(1+\cos^2\theta) \tag{21}$$

for usual dipole transition [27,28]. Here we follow the analytical treatment proposed in Refs. [27,29], which is achieved by adiabatical elimination of the internal DOF and then perturbative expansion of the master equation (20), yielding the rate equation for the population p_n of the nth phonon state:

$$\frac{d}{dt}p_n = p_{n+1}\Gamma_{n+1\to n} + p_{n-1}\Gamma_{n-1\to n} - p_n(\Gamma_{n\to n-1} + \Gamma_{n\to n+1}), \tag{22}$$

where $\Gamma_{n\to m}$ is the transition rate from nth phonon state to mth phonon state.

The transition rates $\Gamma_{n\to n\pm1}$ can be obtained by calculating all possible scattering processes up to the first order of LD parameters [9,10,12], as shown in Fig. 3:

$$\Gamma_{n\to n\pm1} = 2\alpha\gamma\left|\mathcal{T}_n^{\mathcal{D}}\right|^2 + 2\gamma\left|\mathcal{T}_n^{\gamma,\pm}\right|^2 + 2\kappa\left|\mathcal{T}_n^{\kappa,\pm}\right|, \tag{23}$$

with geometry factor $\alpha = \frac{2}{5}$ in dipole transition [29].

The scattering amplitude $\mathcal{T}_n^{\mathcal{D}}$ denotes the diffusion from atomic excitation of the nth phonon, $\mathcal{T}_n^{\gamma,\pm}$ and $\mathcal{T}_n^{\kappa,\pm}$ denote the cooling/heating transitions from the nth phonon steady state $|\psi_n\rangle = |g,0_c,n\rangle$ and then dissipating back to the $n\pm$ 1-th steady states $|\psi_{n\pm1}\rangle = |g,0_c,n\pm1\rangle$ by the spontaneous emission and by the cavity decay, respectively:

$$\mathcal{T}_n^{\mathcal{D}} = \langle\psi_{n\pm1}|W_\gamma^1 G(E_i)V_0^0|\psi_n\rangle,$$
$$\mathcal{T}_n^{\gamma,\pm} = \langle\psi_{n\pm1}|W_\gamma^0 G(E_i)V_0^1|\psi_n\rangle + \langle\psi_{n\pm1}|W_\gamma^0 G(E_i)V_1 G(E_i)V_0^0|\psi_n\rangle,$$

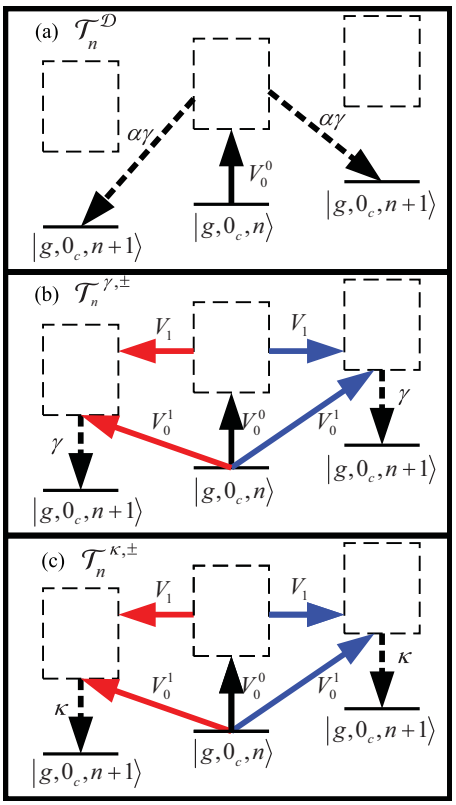

FIG. 3. (Color online) The illustration of cooling and heating processes. The dash rectangle represents the excited subspace. (a) The cooling/heating process due to recoil of the spontaneously emitted photon. (b) The cooling/heating process due to red/blue sideband transitions and dissipation by the spontaneous emission. (c) The cooling/heating process due to red/blue sideband transitions and dissipation by the cavity decay.

$$\mathcal{T}_n^{\kappa,\pm} = \langle\psi_{n\pm1}|W_\kappa G(E_i)V_0^1|\psi_n\rangle + \langle\psi_{n\pm1}|W_\kappa G(E_i)V_1 G(E_i)V_0^0|\psi_n\rangle. \quad (24)$$

Here E_i is the energy of the initial state $|\psi_n\rangle$ and $G(z)$ is defined by [30]

$$G(z) = \frac{1}{z - H_{\text{eff}}}, \quad (25)$$

with the effective Hamiltonian

$$H_{\text{eff}} = H_e - i\kappa a^\dagger a - i\gamma|e\rangle\langle e|. \quad (26)$$

W_γ^0, W_γ^1, and W_κ are the quantum jump operators which denote the dissipation of the system:

$$W_\gamma^0 = |g\rangle\langle e|, \quad W_\gamma^1 = i\tilde{\eta}_g(b^\dagger + b)|g\rangle\langle e|, \quad W_\kappa = a, \quad (27)$$

with the LD parameter $\tilde{\eta}_g$ scaling the mechanical coupling of radiation with the atomic motion and defined by (assuming that $k_g \approx |\boldsymbol{k_{L1}}|$)

$$\tilde{\eta}_g = k_g\sqrt{\frac{1}{2M\nu}} \approx |\boldsymbol{k_{L1}}|\sqrt{\frac{1}{2M\nu}}. \quad (28)$$

Calculating Eq. (24), we get the transition rates

$$\Gamma_{n\to n+1} = (n+1)A_+, \Gamma_{n\to n-1} = nA_-. \quad (29)$$

Here $A_\pm$ are the heating and cooling parameters, respectively,

$$A_\pm = 2\alpha\gamma|\mathcal{T}^D|^2 + 2\gamma|\mathcal{T}^{\gamma,\pm}|^2 + 2\kappa|\mathcal{T}^{\kappa,\pm}|^2, \quad (30)$$

with

$$\mathcal{T}^D = i\tilde{\eta}_g\frac{\Omega_g}{2}\frac{(\Delta_g - \Delta_r)(i\kappa + \delta_c)}{f(0)}, \quad (31)$$

$$\mathcal{T}^{\gamma,\pm} = \frac{\Omega_g}{2}\left[-i\eta_g\frac{(i\kappa \mp \nu + \delta_c)(\mp\nu + \Delta_g - \Delta_r)}{f(\mp\nu)} + \eta_c\tilde{g}^2(\Delta_g - \Delta_r)(\mp\nu + \Delta_g - \Delta_r)\frac{(2i\kappa + 2\delta_c \mp \nu)}{f(0)f(\mp\nu)} - i\eta_r\frac{\Omega_r^2}{4}(i\kappa + \delta_c)(i\kappa \mp \nu + \delta_c)\frac{(\mp\nu)}{f(0)f(\mp\nu)}\right], \quad (32)$$

$$\mathcal{T}^{\kappa,\pm} = \frac{\Omega_g}{2}\left\{-i\eta_g\frac{\tilde{g}(\mp\nu + \Delta_g - \Delta_r)}{f(\mp\nu)} + \eta_c\tilde{g}(\Delta_g - \Delta_r) \times [(i\kappa + \delta_c)(\mp\nu + \Delta_g - \Delta_r)(\mp\nu + i\gamma + \Delta_g) - (i\kappa + \delta_c)\Omega_r^2 + \tilde{g}^2(\mp\nu + \Delta_g - \Delta_r)]\frac{1}{f(0)f(\mp\nu)} - i\eta_r\frac{\Omega_r^2}{4}\tilde{g}(i\kappa + \delta_c)\frac{(\mp\nu)}{f(0)f(\mp\nu)}\right\}, \quad (33)$$

where

$$f(x) = (i\kappa + x + \delta_c)\left[(x + \Delta_g - \Delta_r)(x + i\gamma + \Delta_g) - \frac{\Omega_r^2}{4}\right] - \tilde{g}^2(x + \Delta_g - \Delta_r). \quad (34)$$

Then the rate equation can be written as

$$\frac{d}{dt}p_n = (n+1)A_-p_{n+1} - [(n+1)A_+ + nA_-]p_n + nA_+p_{n-1}. \quad (35)$$

The rate equation for mean phonon number therefore is

$$\frac{d}{dt}\langle n\rangle = -(A_- - A_+)\langle n\rangle + A_+. \quad (36)$$

If $A_- > A_+$, the atom will be cooled to the final phonon number

$$\langle n\rangle_{ss} = \frac{A_+}{A_- - A_+}, \quad (37)$$

and the cooling rate is

$$W = A_- - A_+. \quad (38)$$

In order to find the optimal condition of the cooling scheme, our strategy is first suppressing the heating rate A_+, then maximizing A_-.

The suppression of A_+, as analyzed, is obtained by choosing the parameters under the conditions (17) and (18).

As shown in Refs. [4,9], the maximum of A_- is at

$$\text{Re}\,f(\nu) = 0, \quad (39)$$

which is

$$(\nu - \delta_c)\left[(\nu + \Delta_g - \Delta_r)(\nu + \Delta_g) - \frac{\Omega_r^2}{4}\right] = (\tilde{g}^2 + \kappa\gamma)(\nu + \Delta_g - \Delta_r), \quad (40)$$

where the denominator of A_- is minimized. Physically, $\mathrm{Re}\, f(\nu) = 0$ corresponds to tuning the red sideband transition of "cooling" laser into resonance with a dressed state of the internal excited states.

Then in the good cavity limit, we can calculate $A_\pm$ under the cooling conditions (17), (18), and (39):

$$A_+ = \frac{\kappa^2\Omega_g^2}{2|f(0)|^2}\left[\left(\alpha\tilde{\eta}_g^2 + \eta_r^2\right)\nu^2\gamma + \left(\eta_c^2 + \eta_r^2\right)\tilde{g}^2\kappa\right], \tag{41}$$

$$A_- = \frac{\Omega_g^2}{2}\nu^2\frac{\eta_g^2(\tilde{g}^2\nu)^2 + \left(\frac{-\eta_g+\eta_r}{2}\kappa\frac{\Omega_r^2}{4} + \eta_c\tilde{g}^2\nu\right)^2}{|f(0)|^2(\gamma\nu^2 + \kappa\tilde{g}^2)}. \tag{42}$$

For $A_- \gg A_+$, the final phonon number can be obtained by

$$\langle n\rangle_{ss} \approx \frac{A_+}{A_-} \leqslant \left[\frac{\alpha\tilde{\eta}_g^2 + \eta_r^2}{\eta_g^2}\left(\frac{1}{C}\right) + \frac{\eta_c^2 + \eta_r^2}{\eta_g^2}\left(\frac{\kappa}{\nu}\right)^2\right]\left[\frac{1}{C} + \left(\frac{\kappa}{\nu}\right)^2\right], \tag{43}$$

which can be lower than the order of $O(\frac{1}{C^2} + \frac{\kappa^4}{\nu^4})$.

The corresponding cooling rate is

$$W \approx A_- = \frac{\Omega_g^2}{2}\nu^2\frac{\eta_g^2(\tilde{g}^2\nu)^2 + \left(\frac{-\eta_g+\eta_r}{2}\kappa\frac{\Omega_r^2}{4} + \eta_c\tilde{g}^2\nu\right)^2}{|f(0)|^2(\gamma\nu^2 + \kappa\tilde{g}^2)}. \tag{44}$$

Insert $f(0)$ into Eq. (44), and we get

$$W \approx \frac{\Omega_g^2}{4}\nu^2\frac{\eta_g^2(\tilde{g}^2\nu)^2 + \left(\frac{-\eta_g+\eta_r}{2}\kappa\frac{\Omega_r^2}{4} + \eta_c\tilde{g}^2\nu\right)^2}{\left(\tilde{g}^4\nu^2 + \frac{1}{16}\kappa^2\Omega_r^4\right)(\gamma\nu^2 + \kappa\tilde{g}^2)}. \tag{45}$$

In our scheme, we assume that the strength of the "coupling" laser Ω_r is comparable to $\tilde{g}$, so in the high-finesse cavity limit, $\tilde{g}^2\nu \gg \frac{\kappa\Omega_r^2}{4}$. The cooling rate is about

$$W \approx \frac{\eta_g^2 + \eta_c^2}{2}\frac{\Omega_g^2\nu^2}{\gamma\nu^2 + \kappa\tilde{g}^2}, \tag{46}$$

which is of the same order as in previous cavity cooling [9].

IV. NUMERICAL SIMULATION AND DISCUSSION

It is worthwhile to compare our scheme with the scheme in Ref. [16]. There are several similarities between the two schemes: the two schemes are both achieved in a Λ-type three-level atom coupling with the cavity field and laser fields; in the weak excitation limit, the truncated internal DOF (10) are equivalent to a four-level system in both cases. Moreover, the two schemes can effectively eliminate the heating effects, leading to a lower final temperature than in previous cavity cooling schemes. However, our scheme differs significantly from Ref. [16]. It can be found from the coupling among the internal DOF: in our scheme, states $|g,0_c\rangle$ and $|e,0_c\rangle$ are coupled by the "cooling" laser field, while states $|g,0_c\rangle$ and $|g,1_c\rangle$ are not directly coupled. By contrast, in Ref. [16], states $|g,0_c\rangle$ and $|g,1_c\rangle$ are coupled by a pump laser, while state $|g,0_c\rangle$ is not directly excited to $|e,0_c\rangle$. Thus the level configuration of the internal DOF in our scheme is distinct from the scheme in Ref. [16]. Consequently different heating cancellation mechanisms are employed. In our scheme the heating effects, as analyzed, are suppressed by combination of the CIT effect and the EIT effect; while in Ref. [16], the diffusion and heating transition are suppressed by the property of the cavity standing wave and the cavity-induced EIT, respectively.

The optimal cooling result (43) is determined by the geometry of the experimental setup. In particular, by choosing

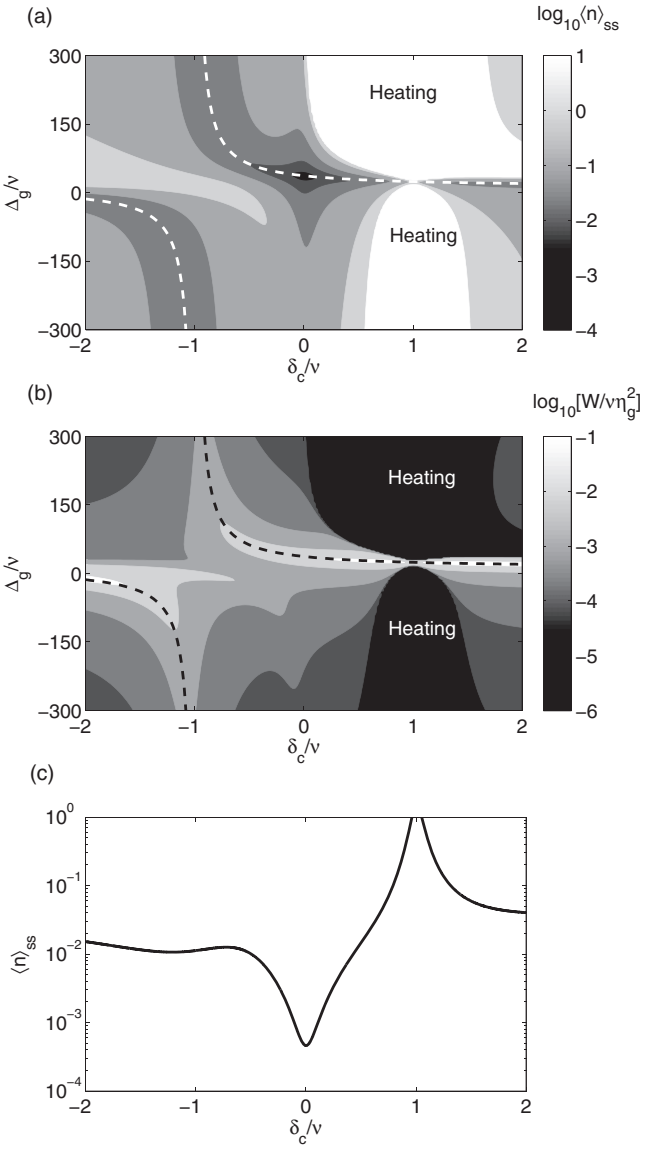

FIG. 4. (a) Contour plot $\log_{10}\langle n\rangle_{ss}$ as a function of δ_c and Δ_g. (b) Contour plot $\log_{10}\frac{W}{\eta_g^2\nu}$ as a function of δ_c and Δ_g. The dashed lines of (a) and (b) correspond to the condition $\mathrm{Re}\, f(\nu) = 0$. (c) The final phonon number as a function of δ_c under the condition $\mathrm{Re}\, f(\nu) = 0$. The other parameters are $\eta_g = \tilde{\eta}_g = 0.1$, $\eta_r = \eta_c = -0.05$, $\phi = \frac{\pi}{3}$, $2\gamma = 10\nu$, $2\kappa = 0.2\nu$ $\Omega_g = \nu$, $\Omega_r = 10\nu$, $g = 10\nu/\sqrt{3}$, $\Delta_r = \Delta_g - \nu$.

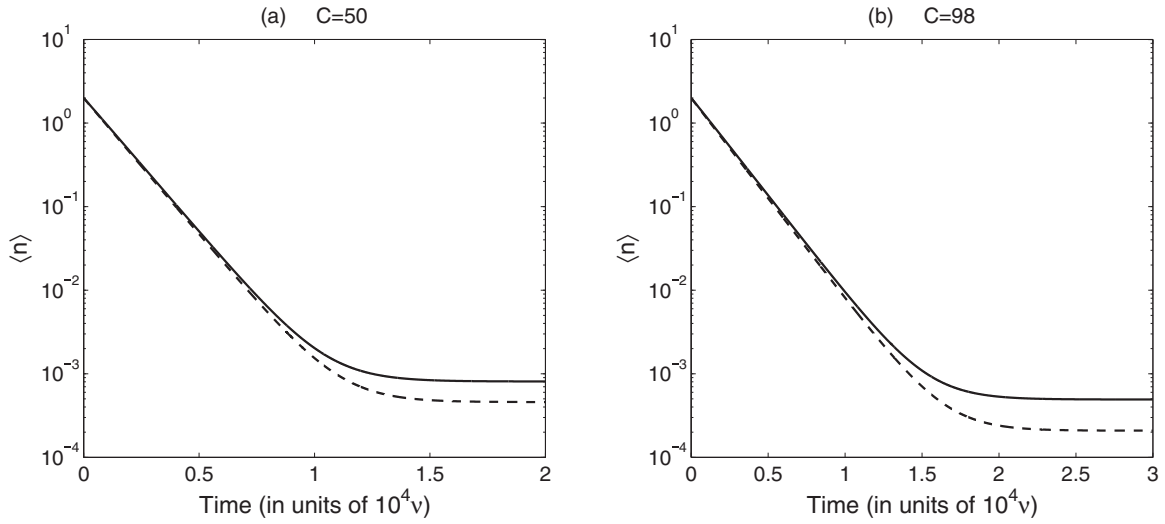

FIG. 5. Numerical simulation of cooling a trapped atom under the cooling conditions (17), (18), and (39). The parameters are $\eta_g = \tilde{\eta}_g = 0.1$, $\eta_r = \eta_c = -0.05$, $\phi = \frac{\pi}{3}$, $2\gamma = 10\nu$, $2\kappa = 0.2\nu$ $\Omega_g = \nu$, $\Omega_r = 10\nu$, (a) $g = 10\nu/\sqrt{3}$, (b) $g = 14\nu/\sqrt{3}$. The dashed lines correspond to the analytical predictions.

the LD parameters

$$\eta_g = \tilde{\eta}_g, \eta_r = \eta_c = 0, \tag{47}$$

which means that the direction of the "cooling" laser is parallel to the motional axis, while the "coupling" laser and cavity axis are perpendicular to the motional axis, the final phonon number can be

$$\langle n \rangle_{ss} < \alpha \frac{1}{C}\left[\frac{1}{C} + \left(\frac{\kappa}{\nu}\right)^2\right]. \tag{48}$$

Compared to the former cavity cooling methods, of the order $O(\frac{1}{C})$, the result of the new scheme can be suppressed by the factor $\alpha[\frac{1}{C} + (\frac{\kappa}{\nu})^2]$.

Figure 4(a) and 4(b) plots the analytical results of the final phonon number and cooling rate as a function of δ_c and Δ_g. The dashed lines correspond to the condition $\mathrm{Re}\, f(\nu) = 0$. From Fig. 4(a) and 4(b), we can see that the regime of lower final phonon number and faster cooling rate is found along the dashed lines, where the cooling transition rate A_- is maximized. Figure 4(c) shows $\langle n \rangle_{ss}$ as a function of δ_c under the condition $\mathrm{Re}\, f(\nu) = 0$. As expected, the minimum value is at $\delta_c = 0$, which coincides with the resonance of the CIT effect.

To verify the analytical result, the numerical simulation of the cooling dynamics is carried out by solving the master equation equation (20) [31]. The result is shown in Fig. 5. For $C = 50$ and $C = 98$, the final phonon numbers are about 8×10^{-4} and 5×10^{-4}, which are lower than than $O(10^{-3})$, while the corresponding the analytical results are about 5×10^{-4} and 2×10^{-4}, respectively. We should note that the analytical treatment has neglected multiphonon processes, so the actual final phonon number is higher than the analytical prediction. Even so, numerical results show that our scheme is still better than previous cavity methods and can achieve the same order as Ref. [16], which is due to successful suppression of the heating effects in our scheme.

From the cooling condition (39), the cooling result is affected by the fluctuations of the "coupling" laser strength Ω_r and the effective coupling $\tilde{g}$. Figure 6 displays the final phonon number as a function of Ω_r by the numerical calculation. As Ω_r deviates 25% of its analytical optimal value, the final phonon number is still of the order $O(10^{-3})$, which is robust against the fluctuation of the "coupling" laser intensity. On the other hand, the effective coupling strength $\tilde{g}$ is determined by both the cavity strength g and the relative position ϕ of the trapped atom in the cavity standing wave. Here we consider the final phonon number affected by the positioning fluctuations when we center the atom at different positions of cavity standing

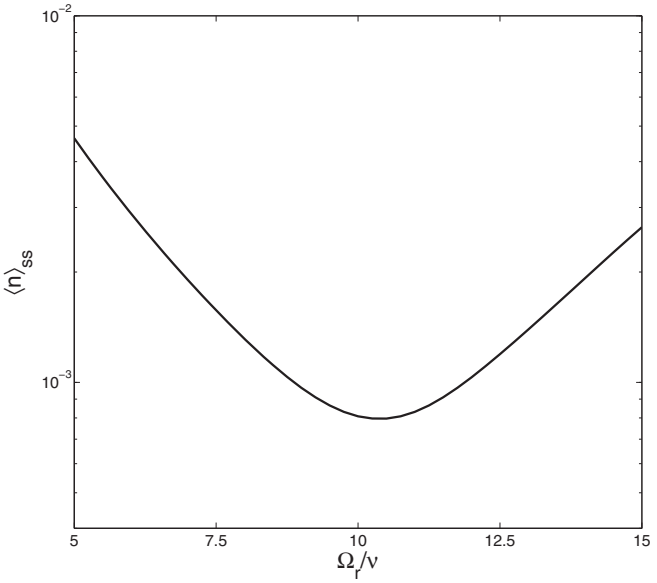

FIG. 6. $\langle n \rangle_{ss}$ as a function of Ω_r, where the optimal value is at $\Omega_{r0} = 10\nu$. The other parameters are $\eta_g = \tilde{\eta}_g = 0.1$, $\eta_r = \eta_c = -0.05$, $\phi = \frac{\pi}{3}$, $2\gamma = 10\nu$, $2\kappa = 0.2\nu$, $\Omega_g = \nu$, $\tilde{g} = 5\nu$, $\Delta_g = 36\nu$, $\Delta_r = 35\nu$, and $\delta_c = 0$.

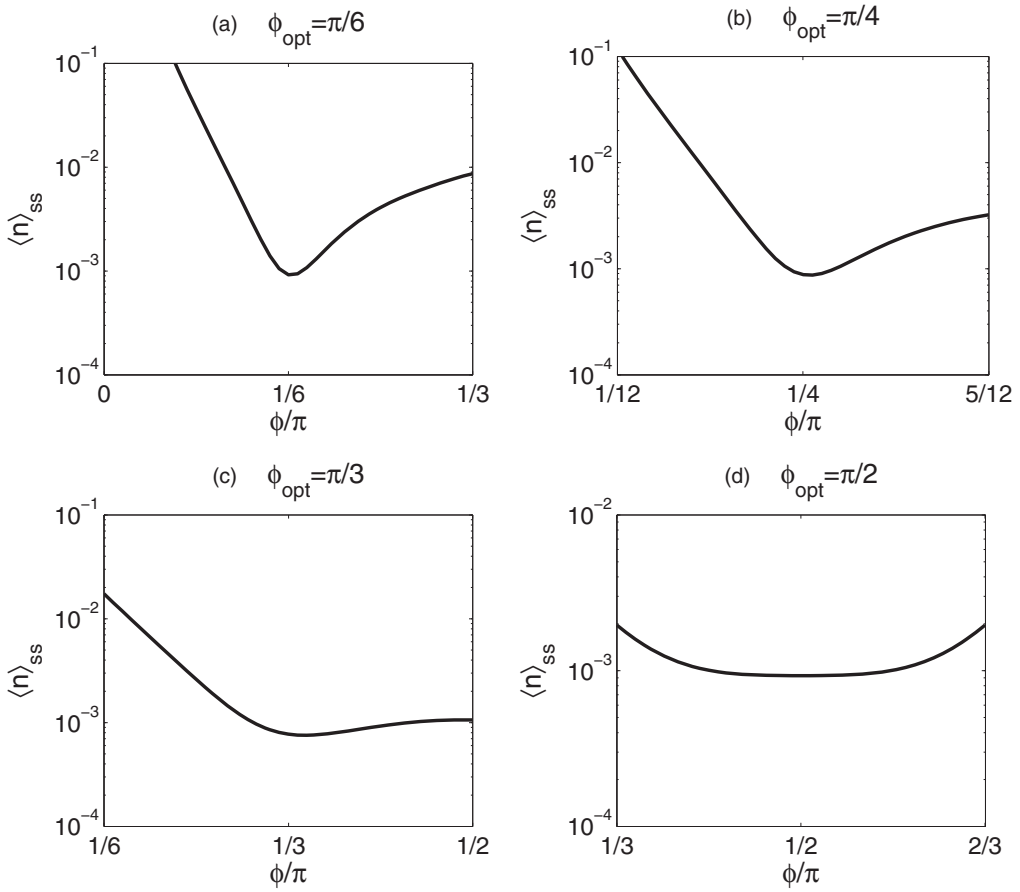

FIG. 7. The final phonon number $\langle n\rangle_{ss}$ as a function of ϕ. For fixed $\tilde{g} = 5\nu$, different situations have been considered: (a) $g = 10\nu$, the corresponding theoretical optimal $\phi_{\rm opt} = \pi/6$; (b) $g = 10\nu/\sqrt{2}$, $\phi_{\rm opt} = \pi/4$; (c) $g = 10\nu/\sqrt{3}$, $\phi_{\rm opt} = \pi/3$; (d) $g = 5\nu$, $\phi_{\rm opt} = \pi/2$. The other parameters are $\eta_g = \tilde{\eta}_g = 0.1$, $\eta_r = \eta_c = -0.05$, $2\gamma = 10\nu$, $2\kappa = 0.2\nu$ $\Omega_g = \nu$, $\Omega_r = 10\nu$, $\Delta_g = 36\nu$, $\Delta_r = 35\nu$, and $\delta_c = 0$.

waves. The numerical calculation of the result is shown in Fig. 7. From Fig. 7 we find that locating the atom at the antinode of the standing wave demonstrates more significant robustness than other situations. Thus for physical realization of the cooling scheme, the atom should be placed near the antinode in the cavity standing wave.

Moreover, simultaneous cooling in three dimensions can be achieved. In LD regime, the cooling dynamics of each dimension can be treated separately. Three-dimensional cooling can be achieved if the cooling conditions (17), (18), and (39) are satisfied in each dimension, which requires that the trapped frequencies along three axis should be similar.

V. SUMMARY

In summary, we have presented the investigation of the cooling dynamics of a Λ configuration trapped atom coupled to a high-finesse optical cavity. The heating effects due to the diffusion and the heating transition can be suppressed simultaneously by combining the cavity-induced transparency and electromagnetically induced transparency effects. By analytical calculation and numerical simulation, we find that the final phonon number of the new scheme can be achieved to the order of $O(\frac{1}{C^2} + \frac{\kappa^4}{\nu^4})$, which is much lower than previous cavity cooling methods. In the future we will investigate the cooling dynamics of many atoms, by taking into account the influence of the collective coupling between the atoms and cavity.

ACKNOWLEDGMENTS

Shuo Zhang would like to thank Xiao-Wei Wang and Jian-Qi Zhang for valuable discussions. This work is supported by the National Natural Science Foundation of China (Grant Nos. 11174370, 61205108, and 11304387), and the Open Project Program of the State Key Laboratory of Mathematical Engineering and Advanced Computing (Grant No. 2013A14).

[1] D. Leibfried *et al.*, Rev. Mod. Phys. **75**, 281 (2003).

[2] C. Monroe, D. M. Meekhof, B. E. King, S. R. Jefferts, W. M. Itano, D. J. Wineland, and P. Gould, Phys. Rev. Lett. **75**, 4011 (1995).

[3] Ch. Roos, T. Zeiger, H. Rohde, H. C. Nagerl, J. Eschner, D. Leibfried, F. Schmidt-Kaler, and R. Blatt, Phys. Rev. Lett. **83**, 4713 (1999).

[4] G. Morigi, J. Eschner, and C. H. Keitel, Phys. Rev. Lett. **85**, 4458 (2000).

[5] J. Cerrillo, A. Retzker, and M. B. Plenio, Phys. Rev. Lett. **104**, 043003 (2010).
[6] S. Zhang, C. W. Wu, and P. X. Chen, Phys. Rev. A **85**, 053420 (2012).
[7] J. P. Zhu, G. X. Li, and Z. Ficek, Phys. Rev. A **85**, 033835 (2012).
[8] S. Zippilli and G. Morigi, Phys. Rev. Lett. **95**, 143001 (2005).
[9] S. Zippilli and G. Morigi, Phys. Rev. A **72**, 053408 (2005).
[10] J. I. Cirac, M. Lewenstein, and P. Zoller, Phys. Rev. A **51**, 1650 (1995).
[11] S. Zippilli, G. Morigi, and W. P. Schleich, J. Mod. Opt. **54**, 1595 (2007).
[12] M. Bienert and G. Morigi, New J. Phys. **14**, 023002 (2012).
[13] M. Bienert and G. Morigi, Phys. Rev. A **86**, 053402 (2012).
[14] P. Domokos and H. Ritsch, J. Opt. Soc. Am. B **20**, 1098 (2003).
[15] P. Horak, G. Hechenblaikner, K. M. Gheri, H. Stecher, and H. Ritsch, Phys. Rev. Lett. **79**, 4974 (1997).
[16] Z. Yi, G. X. Li, and Y. P. Yang, Phys. Rev. A **87**, 053408 (2013).
[17] J. Q. Zhang, Y. Li, and M. Feng, J. Phys.: Condens. Matter **25**, 142201 (2013).
[18] S. Machnes, M. B. Plenio, B. Reznik, A. M. Steane, and A. Retzker, Phys. Rev. Lett. **104**, 183001 (2010).
[19] P. Maunz *et al.*, Nature (London) **428**, 50 (2004).
[20] D. R. Leibrandt, J. Labaziewicz, V. Vuletic, and I. L. Chuang, Phys. Rev. Lett. **103**, 103001 (2009).
[21] M. Wolke *et al.*, Science **337**, 75 (2012).
[22] T. Kampschulte *et al.*, arXiv:1212.3814 [quant-ph].
[23] V. Vuletic, H. W. Chan, and A. T. Black, Phys. Rev. A **64**, 033405 (2001).
[24] T. Blake *et al.*, J. Mod. Opt. **58**, 1317 (2011).
[25] P. R. Rice and R. J. Brecha, Opt. Commun. **126**, 230 (1996).
[26] M. Fleischhauer, A. Imamoglu, and J. P. Marangos, Rev. Mod. Phys. **77**, 633 (2005).
[27] J. I. Cirac, R. Blatt, and P. Zoller, Phys. Rev. A **46**, 2668 (1992).
[28] D. Reiß, A. Lindner, and R. Blatt, Phys. Rev. A **54**, 5133 (1996).
[29] S. Stenholm, Rev. Mod. Phys. **58**, 699 (1986).
[30] C. Cohen-Tannoudji, J. Dupont-Roc, and G. Grynberg, *Atom-Photon Interaction* (Wiley, New York, 1992).
[31] S. M. Tan, J. Opt. B **4**, 424 (1999).